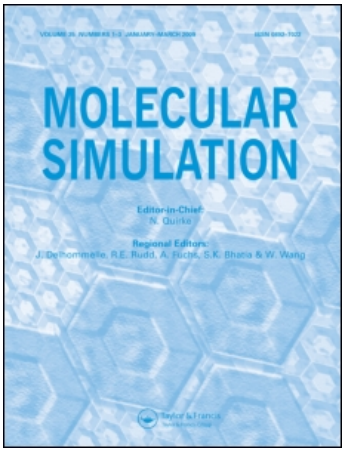

Molecular Simulation
Publication details, including instructions for authors and subscription information:
http://www.informaworld.com/smpp/title~content=t713644482

Monte Carlo Simulation of Binary Gas Adsorption in Zeolite Cavities

Fokion Karavias[a]; Alan L. Myers[a]
[a] Department of Chemical Engineering, University of Pennsylvania, Philadelphia, PA, USA

To cite this Article Karavias, Fokion and Myers, Alan L.(1991) 'Monte Carlo Simulation of Binary Gas Adsorption in Zeolite Cavities', Molecular Simulation, 8: 1, 51 — 72
To link to this Article: DOI: 10.1080/08927029108022467
URL: http://dx.doi.org/10.1080/08927029108022467

Molecular Simulation, 1991, Vol. 8, pp. 51–72
Reprints available directly from the publisher
Photocopying permitted by license only

MONTE CARLO SIMULATION OF BINARY GAS ADSORPTION IN ZEOLITE CAVITIES

FOKION KARAVIAS and ALAN L. MYERS

Department of Chemical Engineering, University of Pennsylvania, Philadelphia, PA 19104, USA

(*Received January 1991, accepted April 1991*)

Grand canonical Monte Carlo simulations have been performed for binary adsorption of Lennard–Jones molecules with point multipole moments in zeolite cavities of type *X*. Fluid–solid electrostatic interactions were taken into account. Phase diagrams and total coverage were calculated for three binaries and compared with experimental measurements. MC simulations gave good agreement with experiment for two mixtures (C_2H_4–CO_2 and CO_2–CH_4) but there were discrepancies between simulation and experiment for the system i-C_4H_{10}–C_2H_4. The dependence of excess Gibbs free energy on the composition and pressure was studied. Negative deviations from ideality are due to energetic heterogeneity and size effects. Unlike liquid–vapor equilibrium, deviations from the Lorentz–Berthelot mixing rules for the adsorbates have little effect upon the phase behavior. Density distributions show that the components compete for the high energy sites inside the cavity; depending on its relative strength of adsorption, one component may be excluded from such positions (CH_4 in CO_2–CH_4), or the two species may share sites inside the cavity (C_2H_4–CO_2).

KEY WORDS: zeolites, adsorption, binary mixtures, Monte Carlo simulations.

INTRODUCTION

Zeolites or molecular sieves are crystalline microporous solids containing cavities and channels of molecular dimensions. Zeolites are widely used in the chemical, biochemical and petroleum industries for adsorptive separation processes and for heterogeneous catalysis. Although other types of adsorbents such as activated carbon have widespread applications, zeolites are dominant in separations of gas and liquid mixtures, gas purification and air separation technology.

Multicomponent adsorption equilibria are needed in the design of equipment for separating mixtures. Over the last few years, significant progress has been made in the understanding of fluid behavior in micropores. However, the prediction of binary adsorption equilibria from single-component isotherm data has been only moderately successful, since thermodynamic models either rely on the assumption of an ideal adsorbed solution or use activity coefficients derived from experimental binary data.

Computer simulations provide a method for studying mixtures in which the intermolecular forces are precisely defined. Simulations have been used to study bulk-phase multicomponent equilibrium and fluid properties in micropores.

Several studies of bulk fluid mixtures have been performed. Gubbins [1] has reviewed the application of several simulation methods in fluid equilibrium. Panagiotopoulos *et al.*, [2,3] studied the phase diagrams of non-ideal fluid mixtures using MC simulations in the canonical and Gibbs ensemble. They performed simulations of

three Lennard-Jones systems and showed how deviations from the Lorentz-Berthelot mixing rules generate highly non-ideal behavior in liquid-vapor equilibrium. Among several other studies, the grand canonical MC method has also been used by Nouacer and Shing [4] to simulate highly non-ideal systems. Mixtures composed of CO_2, naphthalene, and water were considered and the molecules were modeled as Lennard-Jones spheres with point multipole moments.

Heffelfinger *et al.* [5] studied the phase equilibrium of Lennard-Jones mixtures in cylindrical pores. They reported density profiles and phase diagrams for the Ar-Kr mixture in a carbon dioxide pore and compared the simulation results with the density functional theory.

Several studies of single-gas adsorption in zeolites by MC or MD exist in the literature [6–14]. Models such as the spherically-averaged potential for a single isolated faujasite cavity, or detailed approaches based on the atom-atom approximation have been used. In a previous paper [14], we presented MC simulations in the grand canonical ensemble for Lennard-Jones molecules with point multipole moments in zeolite cavities of type *X*. Dispersion-repulsion and electrostatic potentials between the solid and the fluid were taken into account. Thermodynamic and structural properties were calculated for Xe, CH_4, CO_2, C_2H_4, and i-C_4H_{10}. Agreement between simulations and experimental measurements for single-gas isotherms was achieved. Isosteric heats were calculated from ensemble fluctuations and the contributions of individual potentials to the total energy of adsorption was evaluated. The results revealed the importance of adsorbate-adsorbate interactions for sorption in faujasite and verified the large contribution of polar interactions with the electric field generated by the zeolite ions to the total energy of adsorption. Density and energy distributions showed that the cavity may serve either as a relatively homogeneous surface or as a highly heterogeneous one, depending on the molecular characteristics of the adsorbed gas and the type, position, and charge of the zeolite cations.

Although several computer simulations have been performed recently for single-gas adsorption in zeolites, only a few studies of multicomponent adsorption have been reported. Razmus and Hall [11] presented grand canonical MC simulations of N_2, O_2, and their binary mixture in zeolite 5A. They took into account the quadrupole moment of both molecules with a point multipole model and calculated single-gas isotherms and selectivities for the binary mixture.

In this paper we extend our work to multicomponent adsorption in zeolite *X*. The aim of this work is to test the ability of computer simulations to predict binary adsorption in zeolites. These studies provide a powerful tool for identifying the sources of non-idealities observed in zeolite cavities. Furthermore, the simulations serve as model systems for testing thermodynamic or statistical mechanical theories of multicomponent adsorption.

Simulations of three binaries were performed: C_2H_4-CO_2, CO_2-CH_4, and i-C_4H_{10}-C_2H_4 in model zeolite cavities *X*. These binary systems show a rich phase behavior, ranging from ideal to azeotropic. Single-gas isotherms of these systems were reported previously [14].

MODEL AND SIMULATION METHOD

The cavity model developed for single-gas adsorption of CH_4, CO_2, C_2H_4, and i-C_4H_{10} in zeolite *X* is applied to simulation of their binaries. The building blocks of

faujasite are truncated octahedra joined together to form large cavities with a radius of about 7 Å. The oxygen ions forming the walls of the large cavities in zeolite *X* lie roughly in a spherical shell and therefore the zeolite is modeled as a collection of identical, nearly spherical cavities.

In the single-gas simulations we exploited the nearly spherical shape of the zeolite cavity by adopting a spherically-averaged potential for the dispersion and repulsion energies [14,15]:

$$\Psi_{is}^{dr}(r) = 4C\varepsilon_{is}\left[\left(\frac{\sigma_{is}}{R}\right)^{12} L\left\{\frac{r^2}{R^2}\right\} - \left(\frac{\sigma_{is}}{R}\right)^{6} M\left\{\frac{r^2}{R^2}\right\}\right] \tag{1}$$

$$L\{x\} = (1 + 12x + 25.2x^2 + 12x^3 + x^4)/(1 - x)^{10}$$

where

$$M\{x\} = (1 + x)/(1 - x)^4$$

$\Psi_{is}^{dr}(r)$ is a function of r, the radial distance of the adsorbed molecule from the center of the cavity. R is the distance from the center of the cavity to the center of the nearest oxygen atom. For a 13*X* zeolite cavity, $R = 7.057$ Å [15,16]. $(C\varepsilon_{is})$ and σ_{is} are the Lennard–Jones energy and collision parameters of molecule i with the solid wall.

The ions in the zeolite crystal create an electrostatic field **E(r)** inside the cavity that acts upon the adsorbed molecules. The induced electrostatic potential is non-pairwise additive and for a linear molecule has the form [17]:

$$\Psi_i^{ind} = -\left[\frac{\alpha_i}{2} + \frac{1}{3}(\alpha_{\|i} - \alpha_{\perp i})(3\cos^2\theta_i + 1)\right]\mathbf{E(r)}^2 \tag{2}$$

where $\alpha_i = \frac{1}{3}(\alpha_{\|i} + 2\alpha_{\perp i})$ is the average polarizability, $\alpha_{\|i}$ is the polarizability along the internuclear axis, $\alpha_{\perp i}$ is that perpendicular to the internuclear axis and θ_i is the angle between **E(r)** and the vector determining the orientation of the adsorbate molecule. In this model the contribution of the oxygen ions to the electric field **E(r)** is omitted and an effective charge of $z_l = +0.58$ [14] is assigned to the cations closest to the cavity wall. There are 14 cations in a 13*X* cavity and their coordinates are presented in Table 1 [14]. The electric field inside the cavity is calculated as:

$$E^2 = E_x^2 + E_y^2 + E_z^2 \tag{3}$$

where

$$E_q = \sum_l z_l \frac{q_l - q_i}{r^3} \quad \{q = x, y, z\}$$

Table 1 Position and effective charge of cations for the 13*X* zeolite cavity

			Coordinates, Å			
Cation	*No. of sites*	z_l	x	y	z	r
Sodium (II)	4[a]	+ 0.580	3.930	3.930	3.930	6.807
Sodium (III)	10[b]	+ 0.580	− 1.245	6.227	6.227	8.894

[a] 4 ions are placed at (x, y, z), $(x, -y, -z)$, $(-x, y, -z)$ and $(-x, -y, z)$.
[b] 10 ions are placed at $(x, -y, -z)$, $(-x, -y, z)$, $(-x, y, -z)$, (z, x, y), $(z, -x, -y)$, (z, y, x), $(z, -y, -x)$, $(-z, y, -x)$ $(-z, -y, x)$ and $(-z, -x, y)$.

and z_l is the effective charge of the lth cation, q_l is the coordinate of the cation, q_i is the coordinate of a molecule of component i, r is the distance between the cation and the molecule.

For CO_2 and C_2H_4, the contributions of their quadrupole moments with the electrostatic field inside the cavity are taken into account. The potential of a molecule with a point quadrupole moment Q_i interacting with the cavity ions is [17]:

$$\Psi_i^Q = \frac{1}{2}\sum_l z_l Q_i \frac{3\cos^2\theta_{li} - 1}{r^3} \tag{4}$$

where Q_i is the quadrupole moment of the adsorbate, z_l is the effective charge of the cations, and θ_{li} is the angle between the line joining the center of the molecule with the cation and the vector determining the orientation of the adsorbate. The summation is over all the cations of the cavity that are included in the model (14 sodium ions).

The total potential energy of interaction of the molecules with the wall is:

$$\Psi = \Psi^{dr} + \Psi^{ind} + \Psi^Q \tag{5}$$

Dispersion and repulsion adsorbate–adsorbate interactions are modeled by the Lennard–Jones 12–6 potential:

$$U_{ij}^{dr}(r) = 4\varepsilon_{ij}\left[\left(\frac{\sigma_{ij}}{r}\right)^{12} - \left(\frac{\sigma_{ij}}{r}\right)^{6}\right] \tag{6}$$

where ε_{ij} and σ_{ij} are the LJ energy and collision parameters, r is the distance between two adsorbed molecules, and the subscripts refer to components i and j. If $i \neq j$ then the Lorentz–Berthelot mixing rules are used:

$$\sigma_{ij} = \tfrac{1}{2}(\sigma_{ii} + \sigma_{jj}) \tag{7}$$
$$\varepsilon_{ij} = \sqrt{\varepsilon_{ii}\varepsilon_{jj}}$$

The interaction of molecules in neighboring cavities makes a significant contribution to adsorbate–adsorbate energies. It is assumed that the nearest-neighbor cavities are periodic images of the central cavity. The interactions between a molecule in the central cavity and all of its periodic images are taken into account.

Interactions between the quadrupole moments of the CO_2 and C_2H_4 are calculated by:

$$U_{ij}^{QQ} = \frac{3}{4}\frac{Q_iQ_j}{r^5}(1 - 5c_1^2 - 5c_2^2 + 17c_1^2c_2^2 + 2s_1^2s_2^2c_{12}^2 - 16s_1s_2c_1c_2c_{12}) \tag{8}$$

where Q_i and Q_j are the quadrupole moments of the two molecules, $s_i = \sin\theta_i$, $c_i = \cos\theta_i$ and $c_{12} = \cos(\phi_1 - \phi_2)$. The angles θ_i and ϕ_i depend on the relative orientation of the two molecules. Therefore, the total fluid–fluid interaction potential is:

$$U = U^{dr} + U^{QQ} \tag{9}$$

The potential parameters for these simulations are presented in Table 2. The model contains the two adjustable parameters ($C\,\varepsilon_{is}$) and σ_{is} of Equation (1), values of which were obtained by fitting adsorption second virial coefficients to experimental data [14]. The other potential parameters were taken from the literature. No parameters besides those used in the single-gas adsorption are needed for simulation of mixtures.

Table 2 Potential parameters for gases adsorbed in zeolite 13X

Molecule	$C\varepsilon_{is}/k^{a(\alpha)}$ K	$\sigma_{is}^{a(\alpha)}$ Å	ε_{ii}/k K	σ_{ii} Å	α_i $10^{-24}cm^3$	$(\alpha_{\parallel i} - \alpha_{\perp i})$ $10^{-24}cm^3$	Q_i $10^{-26}e.s.u.\ cm^2$
CH_4	12,500	3.375	148.6 [29]	3.82 [29]	2.60 [30]	0.00	0.00
CO_2	15,500	3.375	225.0 [2]	3.80 [2]	2.65 [30]	2.04 [30]	− 4.30 [31]
C_2H_4	15,550	3.430	224.7 [28]	4.163 [28]	4.26 [30]	1.35 [30]	− 3.92 [31]
i-C_4H_{10}	18,800	3.930	330.1 [28]	5.278 [28]	8.32 (*b*)	0.00	0.00

[a] Values obtained from experimental data for adsorption 2nd virial coefficients [14].
[b] Value was calculated by Silberstein method [32].

A series of GCMC simulations of the adsorption of binary mixtures was performed. The algorithm has three steps, Figure 1:

(a) Displacement and Rotation Step. Non-spherical molecules (CO_2 and C_2H_4) are rotated and displaced.

(b) Creation Step. The particle creation is accepted with probability:

$$\mathscr{P} = \min\left[1; \exp\left\{-\frac{\Delta U}{kT} - \ln\frac{(N_i + 1)kT}{y_i PV}\right\}\right] \tag{10}$$

where ΔU is the configurational energy change for creation of a particle, N_i is the current number of molecules of component i in the cavity before the attempted creation, $V\,(=\frac{4}{3}\pi R^3)$ is the volume of the cavity, P is the pressure and y_i is the mole fraction in the ideal gas phase.

(c) Destruction Step. The particle destruction is accepted with probability:

$$\mathscr{P} = \min\left[1; \exp\left\{-\frac{\Delta U}{kT} + \ln\frac{N_i kT}{y_i PV}\right\}\right] \tag{11}$$

The particle creation and destruction steps have been performed to satisfy the condition of microscopic reversibility. First, a random decision was made to create or remove a molecule. Then, the species to be created or destroyed were selected with an equal probability. Microscopic reversibility must apply to the creation and destruction of each component separately.

Four million cycles (each cycle includes the move and creation–destruction steps) were necessary to achieve an acceptable precision in the average composition of the adsorbed phase. The required CPU time on a 2 MFLOPS workstation was 3–10 h, depending on the density of the system. Since the main simulation box was the interior of the zeolite cavity, no more than 13 molecules were present in each configuration and a long Markov chain was needed for good statistics.

Composition and total amount adsorbed are ensemble averages from the simulation of the binary mixture. One attractive feature of GCMC simulations of bulk fluids is that the grand potential Ω and the partition function Ξ can be calculated directly as [18]:

$$-\Omega/kT = \ln \Xi = \langle p\rangle V/kT \tag{12}$$

The pressure p of the bulk liquid is evaluated from intermolecular forces using the virial theorem. In adsorption the grand potential contains an additional term:

$$\begin{aligned}\Omega &= -pV - \pi A \\ &= U - TS - \sum \mu_i N_i\end{aligned} \tag{13}$$

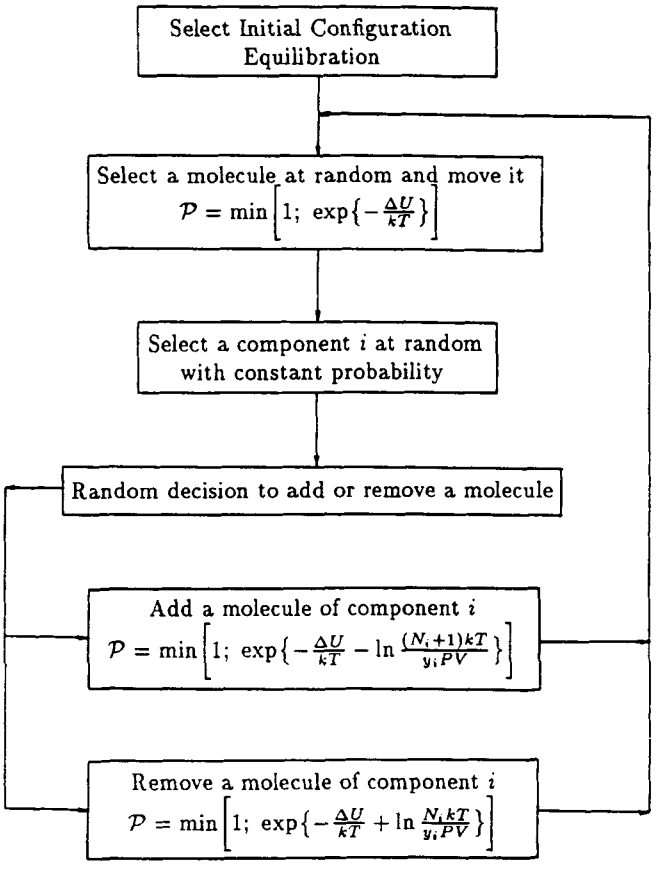

Figure 1 Algorithm for Monte Carlo simulation of a grand canonical ensemble for a mixture.

where π is the surface pressure and A is the surface area of the solid adsorbent. The thermodynamic theory of multicomponent adsorption uses the grand potential as the intensive variable to characterize the standard state. An excess property is defined as the difference between the actual value of the property and the value at the same T and Ω for an ideal solution. For instance, the excess Gibbs free energy of adsorption is:

$$g^e = g(T, \Omega, x_i) - g^{id}(T, \Omega, x_i) \tag{14}$$

The determination of Ω from the simulations is necessary but less straightforward than the calculation of the grand potential for bulk fluids. For planar surfaces, it is possible to break the grand potential $\Omega = -pV - \pi A$ into volume and area terms and calculate each of them as an ensemble average using the virial method [19]. In the case of spherical surfaces, the surface pressure π and the area A depend on the position of the Gibbs dividing surface and although Ω is well-defined, its breakdown into pV and πA is arbitrary. Therefore, the calculation of π and p via the virial method cannot be performed without ambiguity. McQuarrie and Rowlinson [20] have studied the problem of calculating surface pressure using statistical methods and they found that

when the boundary solid has an "ideal" planar surface (i.e. $u(z) = \infty$ at $z < 0$, $u(z) = 0$ at $z \geqslant 0$) pV and πA can be calculated individually. But if the solid is a source of intermolecular potentials there is no unique way of dissecting Ω into volume and area terms. If the adsorption system is both curved and 'non-ideal' as a zeolite cavity, one must work directly with the entity Ω [20,21].

A second route to the grand potential Ω is the direct calculation of the grand partition function:

$$-\Omega/kT = \ln \Xi \tag{15}$$

The grand canonical partition function is a multidimensional integral and its configurational part is an ensemble average:

$$\Xi^{\text{conf}} = \frac{1}{\langle \exp [\beta(U - \Sigma_i \mu_i N_i)] \rangle} \tag{16}$$

However, this calculation introduces new problems similar to those encountered in the determination of Helmoltz free energy from canonical MC simulations. GCMC is designed to sample regions in which the quantity $(U - \Sigma_i \mu_i N_i)$ is either negative or small and positive. Since these regions contribute little to the average of Equation (16), this route to Ω is impractical unless special techniques like umbrella sampling [18] can be applied.

Since it is difficult to obtain Ω directly from the computer simulation, a thermodynamic approach based on the Gibbs adsorption equation [22] is necessary:

$$-d\left(\frac{\Omega}{kT}\right) = N_T \, d \ln P + \sum_i N_T x_i d \ln y_i \quad (T = \text{const}) \tag{17}$$

where N_T is the total amount adsorbed, P is the pressure of the ideal bulk phase, and x_i and y_i are the composition of the adsorbed and bulk phases, respectively. To evaluate the grand potential at any point in multicomponent space, the Gibbs equation has to be integrated at constant temperature from $P = 0$ (where $\Omega \equiv 0$) to the pressure and composition of the point in question. This method is effective if enough simulation points are available and if an extrapolation to $y_i = 0$ or $P = 0$ can be made with acceptable accuracy. The procedure is the same for calculating Ω from experimental data.

The excess Gibbs free energy is a measure of the non-ideal behavior of the binary mixture. Since the chemical potentials μ_i are input parameters in the grand canonical ensemble, g^e can be obtained from Equation (14) as:

$$g^e/RT = (x_1\mu_1 + x_2\mu_2) - (x_1\mu_1^0 + x_2\mu_2^0) - (x_1 \ln x_1 + x_2 \ln x_2) \tag{18}$$

where x_i is the mole fraction in the adsorbed phase, μ_i is the chemical potential of component i in the mixture, and μ_i^0 is the chemical potential i for single-gas adsorption at the same standard state (T,Ω) as those of the binary.

The accuracy of the GCMC simulation for binary mixtures can be checked by performing a thermodynamic integral consistency test which for an ideal gas phase is [22]:

$$\frac{(\Omega_2 - \Omega_1)}{kT} = \int_0^1 \left(\frac{N_1}{y_1} - \frac{N_2}{y_2}\right) dy_1 \quad (T, P = \text{const.}) \tag{19}$$

where Ω_i is the grand potential of pure component i, N_i is the number of adsorbed molecules of i, and y_i is the composition of the ideal gas phase. The integral in

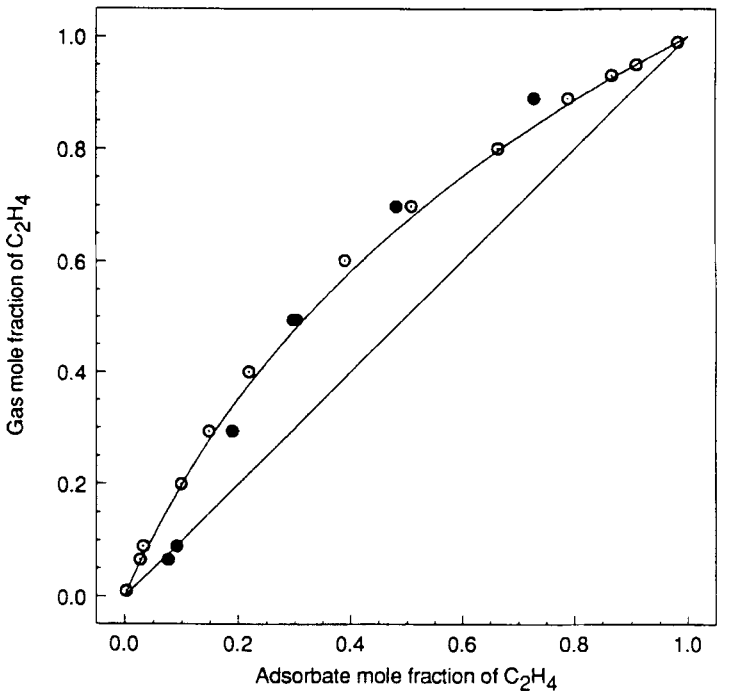

Figure 2 Equilibrium composition diagram for the C_2H_4–CO_2 mixture in 13*X* zeolite at 137.8 kPa and 298.15 K. (○) MC results; (●) experimental measurements of Hyun and Danner; (—) IAS prediction.

Equation (19) is calculated numerically. The simulations of the three binaries were tested for their thermodynamic consistency with respect to the single component adsorption.

RESULTS AND DISCUSSION

Adsorption of Mixtures with Components of Similar Molecular Characteristics; Model Binary C_2H_4–CO_2

C_2H_4 and CO_2 molecules are modeled as a Lennard–Jones sphere containing a point quadrupole moment at the center, Equations (6)–(9). The two components of the mixture have similar values of quadrupole moment and intermolecular potential parameters. Equations (1)–(5) are used for the fluid–solid interactions. The single-gas adsorption simulation gave reasonably good agreement with experiment for CO_2 but average deviations were about 25% for C_2H_4 [14]. The result of the integral consistency test is presented in Table 3: the difference between the right and left hand side of Equation (19) with respect to the grand potential of the more strongly adsorbed component is 1.3%.

The phase diagram of the binary mixture calculated by MC simulations is plotted in Figure 2 and compared with experimental measurements of Hyun and Danner [23] for C_2H_4–CO_2 adsorbed in zeolite 13*X*. The predictions of the Ideal Adsorbed Solution (IAS) theory [24] based on the simulated single-gas isotherms are also

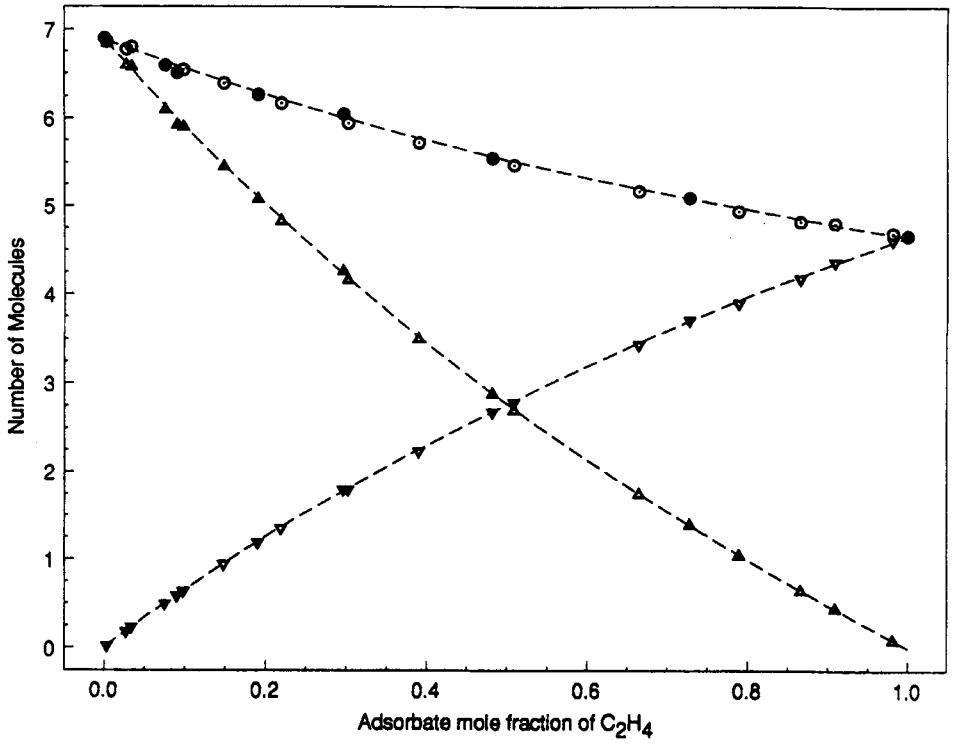

Figure 3 Average occupancies for the C_2H_4–CO_2 mixture in 13*X* zeolite at 137.8 kPa and 298.15 K. (○), (▽) and (△) MC results for total, ethylene and carbon dioxide coverage, respectively; (●), (▼) and (▲) experimental measurements of Hyun and Danner; (– –) IAS predictions.

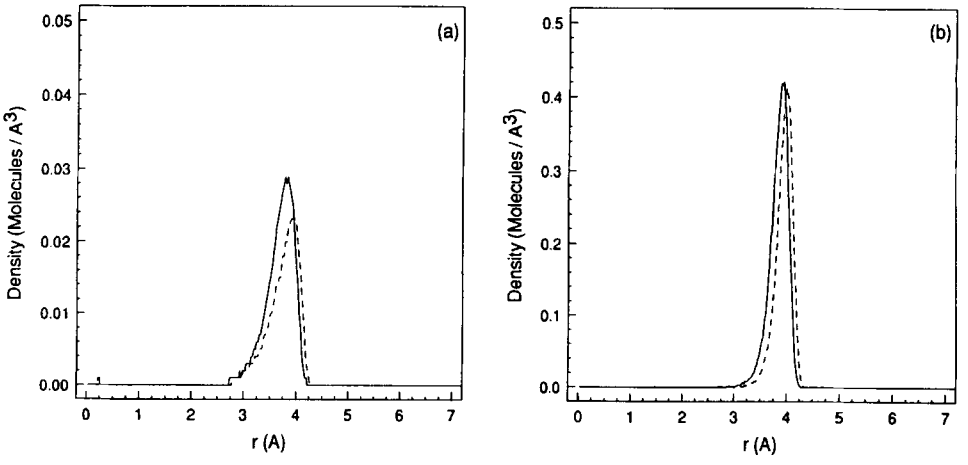

Figure 4 Density profiles as a function of the radius of a 13*X* cavity. (– – –) CO_2, (——) C_2H_4. (a) Angle-averaged density; (b) Local density at fixed angles facing each of the four sodiums II. ($N_{C_2H_4}$ = 2.9, N_{CO_2} = 2.5).

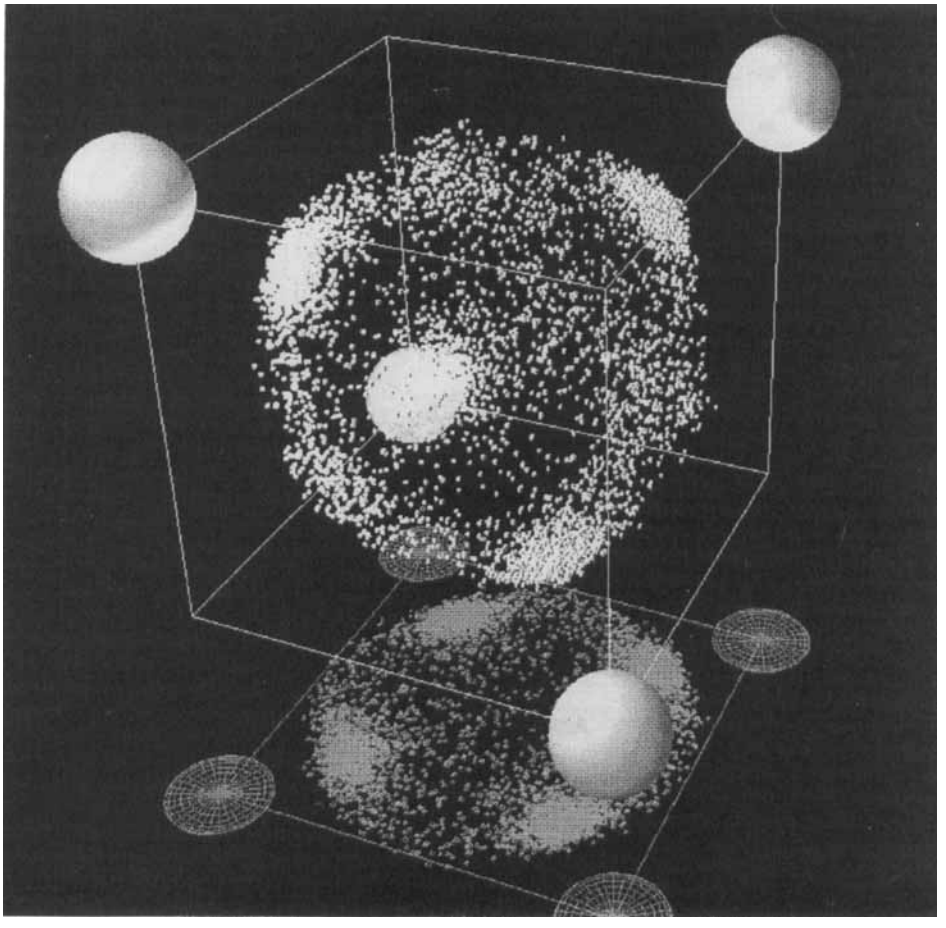

Figure 5 (*See* Color Plate IV) Density distribution of C_2H_4-CO_2 binary in a zeolite cavity of type *X*. The four cations II are located at the corners of a cube at a distance of 6.8 Å from the center of the cavity. Each spot inside the cube represents the position occupied by the center of mass of the adsorbed molecule at different MC steps. C_2H_4 molecules are yellow and CO_2 molecules are red. ($N_{C_2H_4}$ = 2.9, N_{CO_2} = 2.5.)

presented in Figure 2. The experimental data show an azeotrope at $y_1 = 0.09$ which is not predicted by the simulation. However, there is quantitative agreement between simulation and experiment at higher mole fractions of C_2H_4. The selectivity of the zeolite for CO_2 is small (2.5) since carbon dioxide and ethylene have similar molecular properties.

In Figure 3, the coverage of both components is plotted versus the mole fraction of C_2H_4 in the adsorbed phase. Simulation results, experimental measurements, and the IAS predictions are in close agreement. Therefore, GCMC calculations for the mixture predicted the mixture adsorption from single-gas adsorption potentials without using any additional parameters. Although the agreement between simulation and experiment was quantitative for the total loadings, some deviations exist in the *X*–*Y* phase diagram at low mole fraction of C_2H_4 (Figure 2). IAS

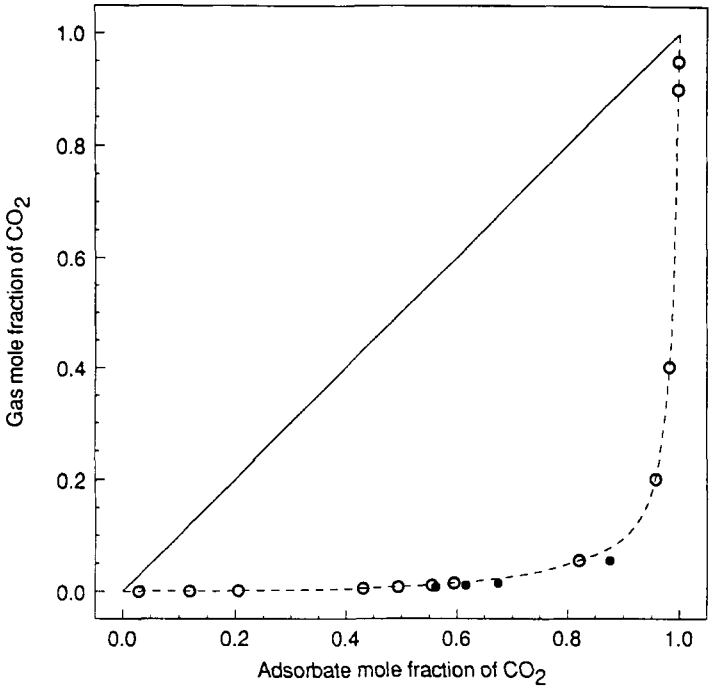

Figure 6 Equilibrium composition diagram for the CO_2–CH_4 mixture 13*X* zeolite at 2,000 kPa and 298.15 K. (○) MC results; (●) experimental measurements of Rolniak and Kobayashi; (- - -) interpolation of the MC results.

predictions agree very well with the simulation data because the two molecules have similar potentials. In the case of single-gas adsorption, the two molecules have very similar density distribution functions and similar curves for the isosteric heat [14].

The density profiles have been calculated from the MC simulations at $y_1 = 0.70$. In Figure 4a the angle-averaged density is presented. The local density in solid angles of 0.04 steradians facing the four cations II (where energy minima are located) is plotted in Figure 4b. Both components are concentrated at high energy sites near these cations because of the electrostatic interactions with the electric field. The localization effect can be seen by comparing Figure 4a and 4b; the density of both components along the axis that connects the center with the cations II is 15–20 times higher than the angle-averaged density.

The spatial distributions of the adsorbed molecules is shown in the 3-D diagram, Figure 5. The four sodium ions II are located 6.8 Å from the center of the cavity at the corners of a cube. The positions occupied by ethylene and carbon dioxide molecules over 1,000 MC steps selected randomly during the simulation are presented. Ethylene and carbon dioxide are distributed similarly in binary adsorption. The two components compete for positions close to the four sodiums but neither molecule has an advantage. At this coverage (5.4 molecules/cavity), the four energy sites are saturated and some molecules of C_2H_4 and CO_2 are displaced to less energetically favorable positions.

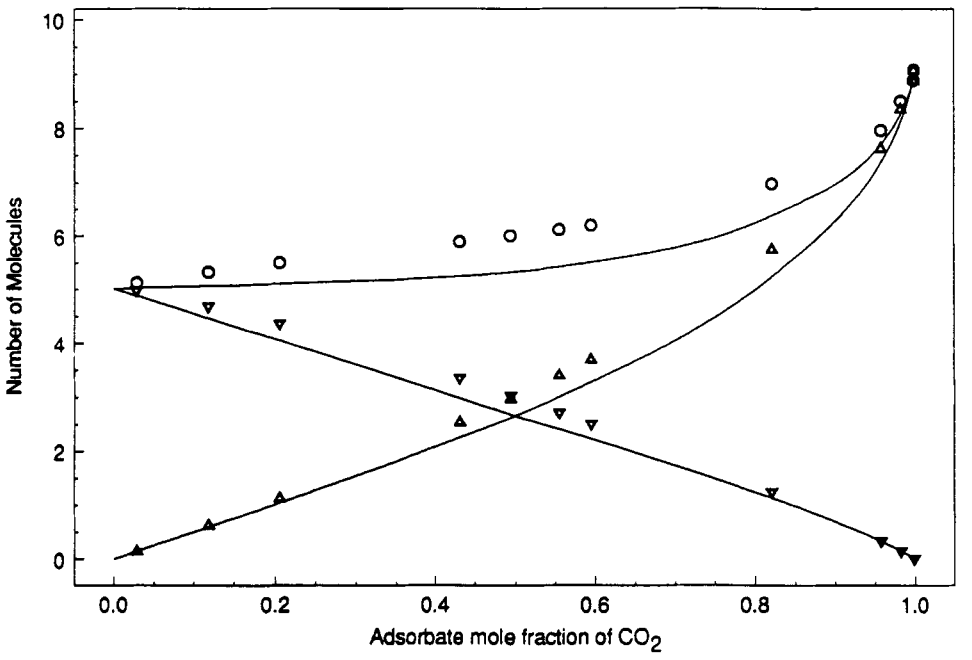

Figure 7 Average occupancies for the CO_2–CH_4 mixture in 13*X* zeolite at 2,000 kPa and 298.15 K. (○), (▽) and (△) MC results for total, methane and carbon dioxide coverage, respectively. (—) IAS predictions.

Adsorption of Mixtures with Polar and Non-Polar Components; Model Binary: CO_2–CH_4

Simulations of the binary mixture CO_2–CH_4 adsorbed in zeolite cavities of type *X* were performed. The two molecules are about the same size. Simulations of the single-gas adsorption have shown that the zeolite cavity is almost homogeneous surface for CH_4 but is highly heterogeneous for CO_2. The results of an integral consistency test of the MC simulations are shown in Table 3. The deviation between the right and left hand side of Equation (19) with respect to the grand potential of the more strongly adsorbed component was 0.5%.

The phase diagram for the binary mixture is presented in Figure 6. Simulation results are compared with experimental measurements of Rolniak and Kobayashi [25]. The shape of the diagram reveals the high selectivity of faujasite for carbon dioxide due to its quadrupole interactions with the electric field. There is good

Table 3 Thermodynamic consistency test of the MC simulations at $T = 298$ K

Binary	*P kPa*	$-\Omega_1/kT$	$-\Omega_2/kT$	$(\Omega_2 - \Omega_1)/kT$	*Integral eqn. (19)*
C_2H_4–CO_2	138	18.2	22.4	−4.2	−4.5
CO_2–CH_4	2,000	44.1	8.8	35.3	35.5
i-C_4H_{10}–C_2H_4	138	17.4	18.3	−0.9	−0.6

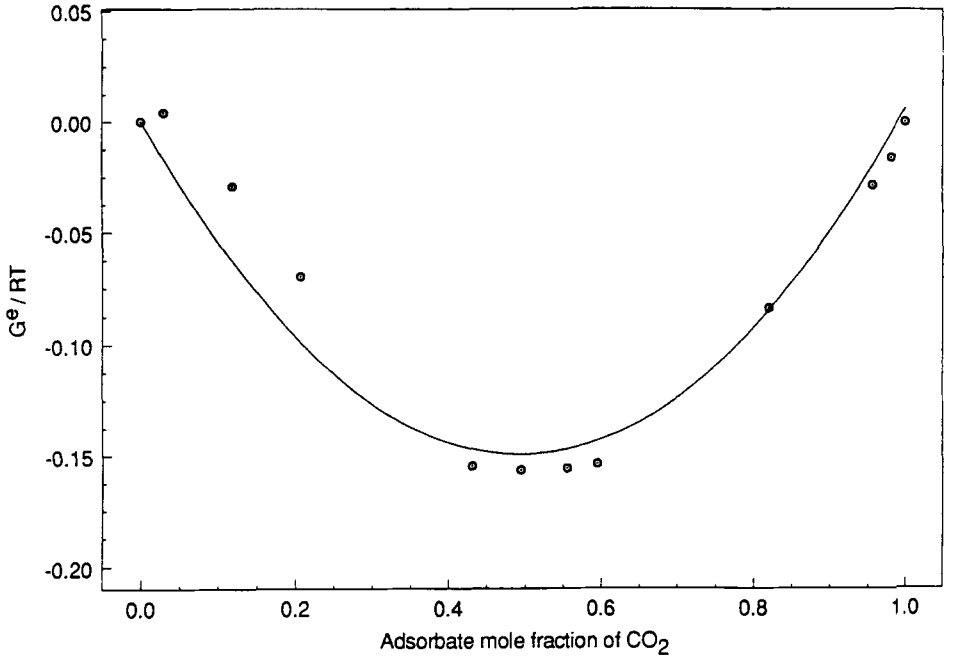

Figure 8 Excess Gibbs free energy of the adsorbed phase for the CO_2–CH_4 mixture in 13*X* zeolite at 2,000 kPa and 298.15 K. The solid line is a quadratic polynomial fit of the points.

agreement between simulations and experimental data. No parameters other than those of the single-gas potentials were used for simulation of the binary adsorption. In the MC simulations, the gas phase was considered ideal, Equations (10)–(11). At $y_{CO_2} = 0.5$, the fugacity coefficient of carbon dioxide in the gas phase is 0.95; therefore the error due to substitution of partial pressure for fugacity is 5%. However, the consistency test in Table 3 is based on an integral and there is a cancellation of errors [22].

Simulations of bulk fluid mixtures have shown that deviations from the Lorentz–Berthelot mixing rules, equation (7), generate non-ideal behavior in liquid-vapor equilibria [2]. In order to examine the effect of these deviations on the phase diagram of adsorption systems, simulations have been performed for the unlike pair potential defined by:

$$\varepsilon_{ij} = \sqrt{\varepsilon_{ii}\varepsilon_{jj}}(1 - k_{ij}) \tag{20}$$

In the case of liquid-vapor equilibria, values of the parameter $|k_{ij}| > 0.15$ produce large deviations from ideality in bulk mixtures including phase splitting. Simulations of the CO_2–CH_4 binary in zeolite cavities for $k_{ij} = \pm 0.20$ have been performed and results for two mixtures are presented in Table 4. It is seen that the adsorbed-phase composition is insensitive to k_{ij}. The fluid–fluid unlike-pair interactions do not affect the behavior of the adsorbed phase significantly because the solid–fluid potentials accounts for more than 80% of the total energy of adsorption [14].

MC results for the individual and total loadings are compared with the predictions of the Ideal Adsorbed Solution theory (IAS) in Figure 7. IAS predictions are based on the simulations of the single-gas isotherms of CO_2 and CH_4 [14] and underestimate

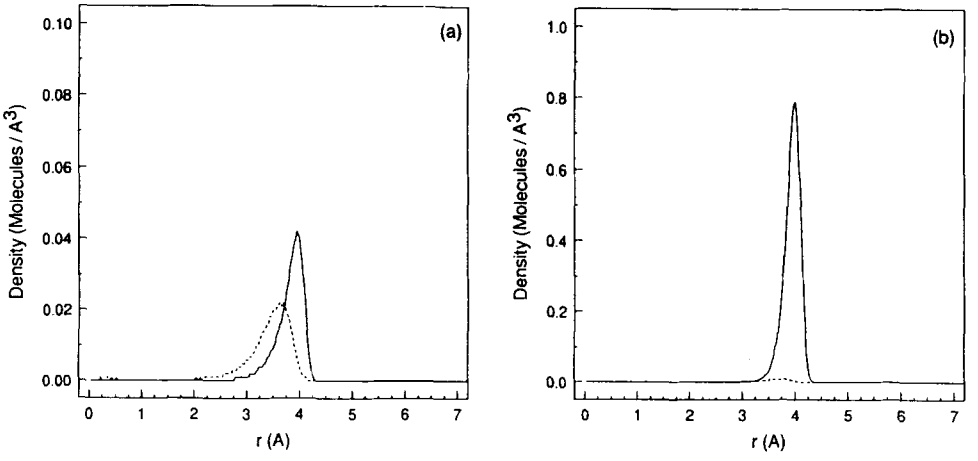

Figure 9 Density profiles as a function of the radius of a 13*X* cavity. (- - -) CH_4, (——) CO_2. (a) Angle-averaged density; (b) Local density at fixed angles facing each of the four sodiums II. (N_{CO_2} = 3.7, N_{CH_4} = 2.5).

the average occupancy of both CO_2 and CH_4. Deviations from ideality are negative, as observed for many multicomponent adsorption systems [26].

Excess Gibbs free energy has been calculated for the MC results by Equation (18). g^e is a function of both the composition of the adsorbed phase and the grand potential Ω. In Figure 8, g^e is plotted versus the mole fraction of CO_2 in the adsorbed phase; at 2,000 kPa the grand potential (Ω/kT) varies from 10 to 25 as x_1 increases from 0 to 1. The excess Gibbs free energy is approximately quadratic in composition and its magnitude indicates small negative deviations from Raoult's law ($\gamma^x = 0.5$). Among the several factors which may influence multicomponent adsorption, the most important are:

(a) Adsorbate–adsorbate molecular interactions.
(b) Effects of energetic heterogeneity caused by variations in the chemical composition of the surface.
(c) Entropic effects due to difference in sizes of adsorbate molecules.
(d) Exclusion effects in which small molecules are adsorbed but large ones are excluded from the cavity.

Table 4 Effect of unlike-pair fluid–fluid interactions on the adsorbed phase composition

Binary	y_1	x_1		
		$k_{12} = +0.2$	$k_{12} = 0.0$	$k_{12} = -0.2$
CO_2–CH_4	0.0005	0.131	0.118	0.162
	0.0077	0.517	0.494	0.488
	0.0550	0.841	0.821	0.773
i-C_4H_{10}–C_2H_4	0.0500	0.192	0.234	0.267
	0.6000	0.523	0.513	0.505
	0.9500	0.742	0.708	0.675

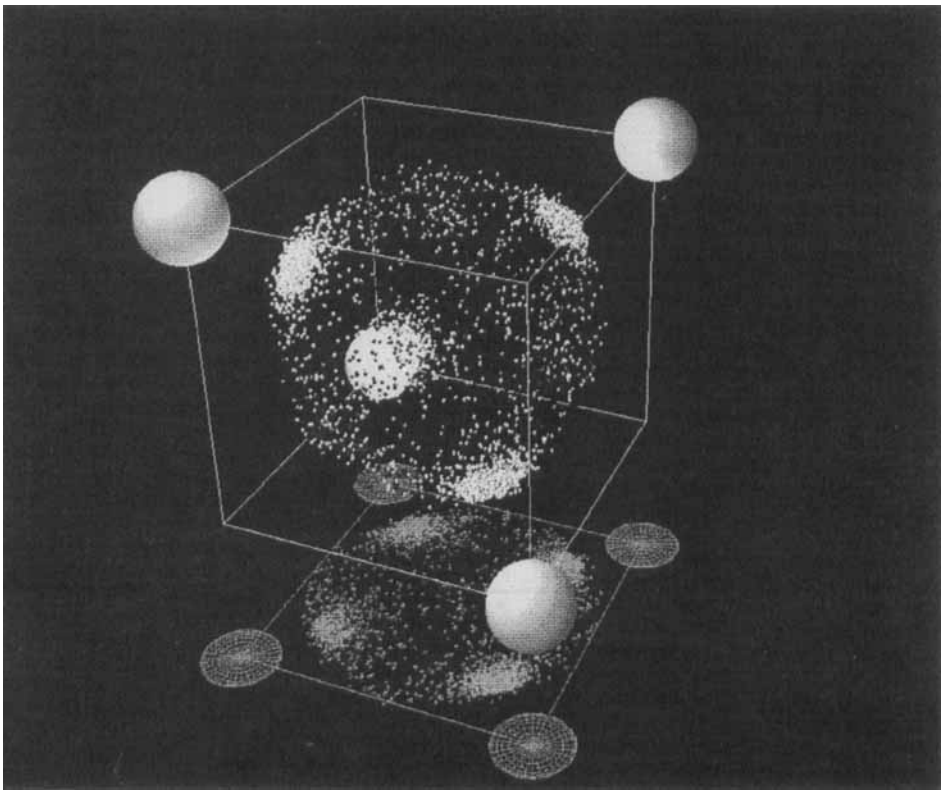

Figure 10 (*See* Color Plate V) Density distribution of CO_2-CH_4 binary in a zeolite cavity of type *X*. The four cations II are located at the corners of a cube at distance of 6.8 Å from the center of the cavity. Each spot inside the cube represents the position occupied by the center of mass of the adsorbed molecule at different MC steps. CO_2 molecules are red and CH_4 molecules are blue. (N_{CO_2} = 3.7, N_{CH_4} = 2.5.)

For the binary CO_2–CH_4 the effect of energetic heterogeneity is responsible for the observed negative devations. The unlike-pair adsorbate–adsorbate interactions are nearly ideal and entropic effects are small since CO_2 and CH_4 molecules are about the same size.

In Figure 9a-b, density profiles for a simulation of the CH_4–CO_2 binary mixture at x_1 = 0.595, 2,000 kPa and 298.15 K are presented. At these conditions, the filling of both components is moderate (N_{CO_2} = 3.7 and N_{CH_4} = 2.5). Figure 9a shows the angle-averaged density as a function the cavity radius. The local density along angles of 0.04 steradians facing the four cations II is plotted in Figure 9b. Carbon dioxide is highly concentrated at these positions because of the interaction of its large quadrupole moment with the electric field generated by the sodium ions, but the density of methane is almost zero.

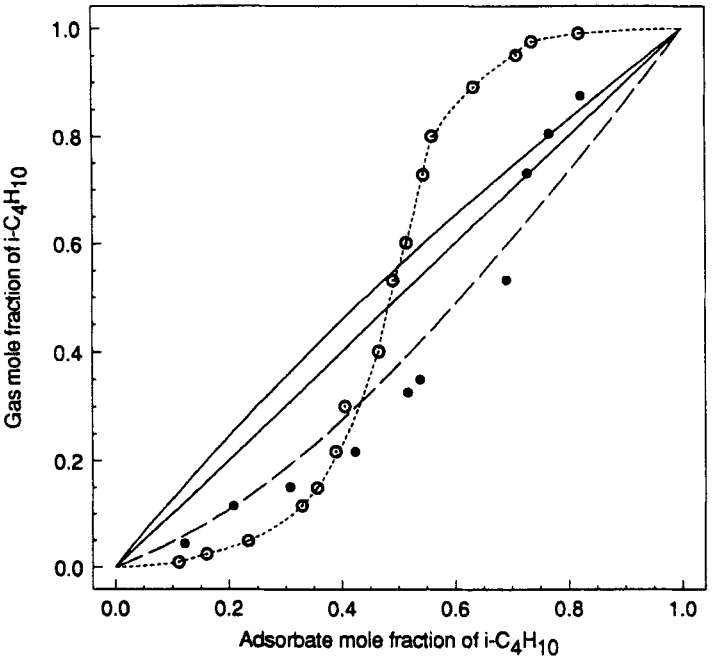

Figure 11 Equilibrium composition diagram for the i-C_4H_{10}–C_2H_4 mixture in 13X zeolite at 137.8 kPa and 298.15 K. (○) MC results; (●) experimental measurements of Hyun and Danner; (——), (– –) IAS predictions from simulated and experimental signal-gas isotherms, respectively; (– – –) interpolation of the MC results.

The spatial distribution of the adsorbed molecules is shown in the 3-D diagram, Figure 10. Although in the case of single-gas adsorption, methane molecules are uniformly distributed inside a spherical shell [14], in binary adsorption CH_4 is excluded by the carbon dioxide molecules from positions close to the sodium ions.

In summary, carbon dioxide and methane molecules compete inside the zeolite cavity for sites of minimum energy. As the density profiles reveal, CO_2 is more strongly adsorbed and displaces methane to less energetically favorable sites.

Adsorption of Mixtures with Components of Different Size; Model Binary i-C_4H_{10}–C_2H_4

Isobutane is an almost spherical molecule with a small permanent dipole moment (0.1 D) and a large polarizability. Since the dipole contributes less than 1% of the total energy of adsorption, it has been neglected and the molecule is modeled as a Lennard–Jones sphere, Equations (1–2), (6). Simulations of the binary i-C_4H_{10}–C_2H_4 adsorbed in zeolite X were performed at several pressures at 298.15 K. The size ratio $\sigma_1/\sigma_2 = 1.3$ of the two molecules introduces large entropic effects that influence the phase behavior dramatically. The integral consistency test for the MC simulations in Table 3 shows an error of 1.6%.

The phase diagram for this binary is compared with experimental data of Hyun and Danner [23] in Figure 11. Both the experimental data and the simulations show an

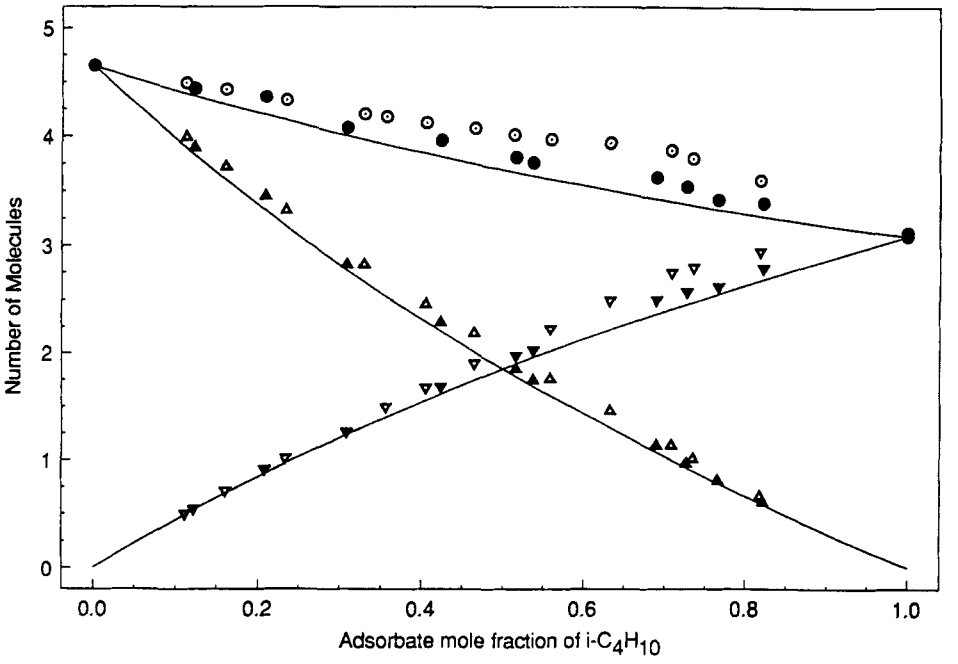

Figure 12 Average occupancies for the i-C_4H_{10}–C_2H_4 mixture in 13X zeolite at 137.8 kPa and 298.15 K. (⊙), (▽) and (△) MC results for total, isobutane and ethylene coverage, respectively, (●), (▼) and (▲) experimental measurements of Hyun and Danner; (——) IAS predictions.

azeotrope. Two lines are calculated from the single-gas isotherms using Ideal Adsorbed Solution theory: the upper IAS line is from the simulated isotherms and the lower IAS line is from the experimental isotherms. The difference is due to a systematic deviation of about 25% between simulations and experiment for the ethylene isotherm [14]. If the discrepancy were removed, the IAS predictions would coincide and the requirements of thermodynamic consistency would force S-shaped curve for the simulations to agree with the S-shaped curve from experiment.

The individual and total loadings obtained from the simulations are compared with experiment in Figure 12. The solid lines are the IAS predictions based on simulation data for the single gases. IAS underestimates the amount adsorbed, which implies negative deviations from Raoult's law. The g^e diagram in Figure 13 shows that the negative deviations are large. Simulations were performed for values of the parameter $k_{ij} = \pm 0.2$ in Equation (20) and the results in Table 4 shows that nonidealities of fluid–fluid interactions are not responsible for the deviations from Raoult's law, which assumes that the composition of the adsorbed phase is homogeneous. The difference in size and polarity of the two molecules affects the energy of their interaction with the zeolite cavity and induces a segregation of the molecules within the cavity. IAS theory does not consider local variations in composition.

To show the dependence of g^e on P, the quantity $F = g^e/RT/(x_1 x_2)$ is plotted versus the grand potential Ω/kT in Figure 14. It is assumed that g^e is approximately quadratic in composition and therefore F is a weak function of the adsorbed phase mole fraction. The data are fitted by an exponential expression proposed by Myers and

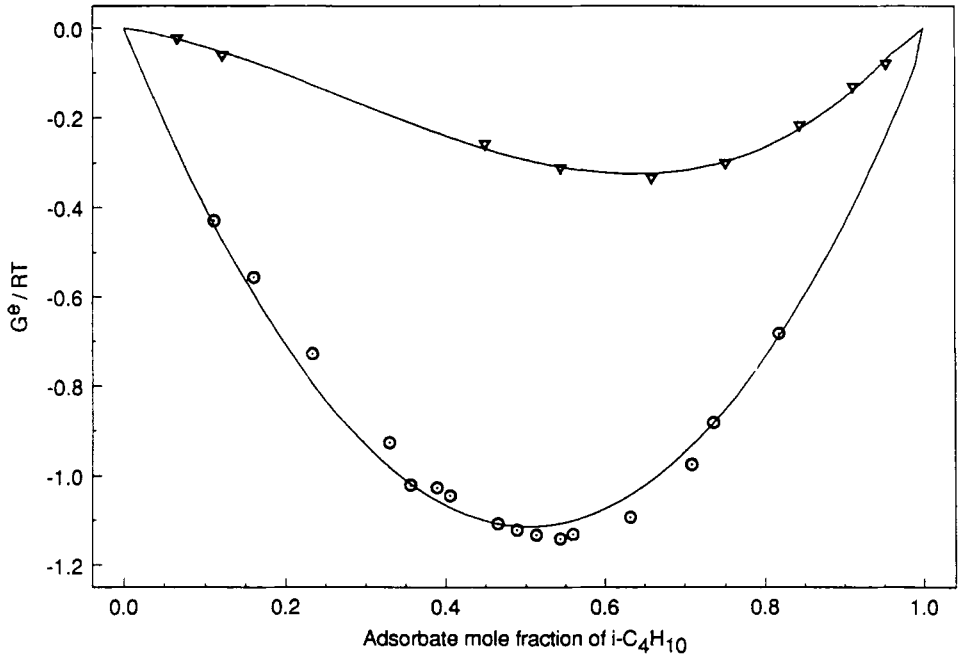

Figure 13 Excess Gibbs free energy of the adsorbed phase for the i-C_4H_{10}–C_2H_4 mixture in 13X zeolite at 298.15 K. (○) P = 137.8 kPa; (▽) P = 1 kPa. The solid lines are polynomial fits.

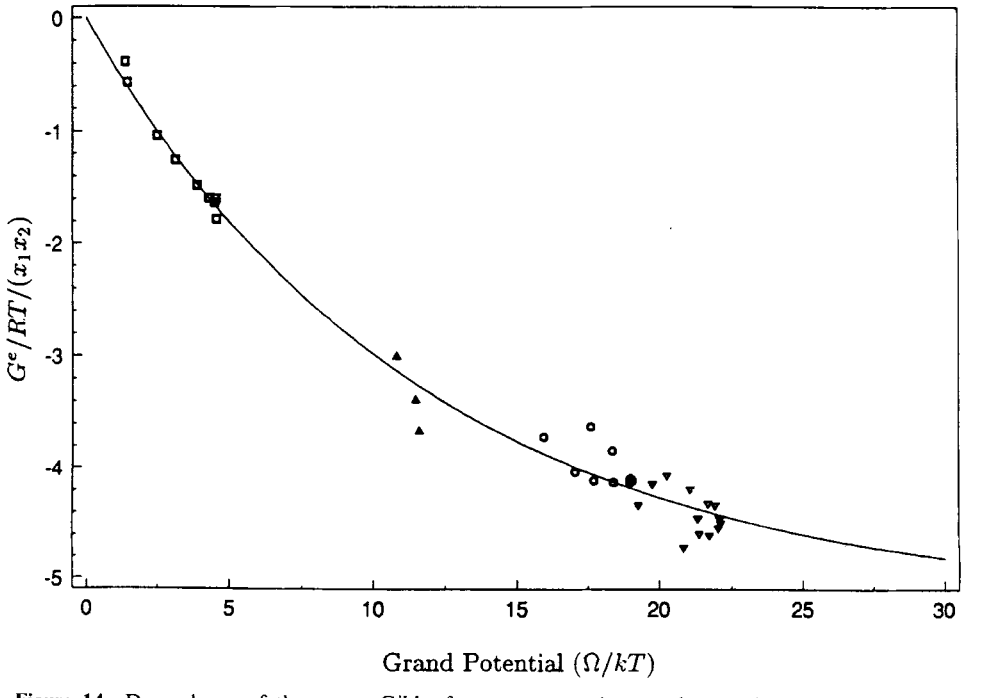

Figure 14 Dependence of the excess Gibbs free energy on the grand potential. (□) P = 1 kPa; (△) P = 10 kPa; (○) P = 70 kPa; (▽) P = 137 kPa.

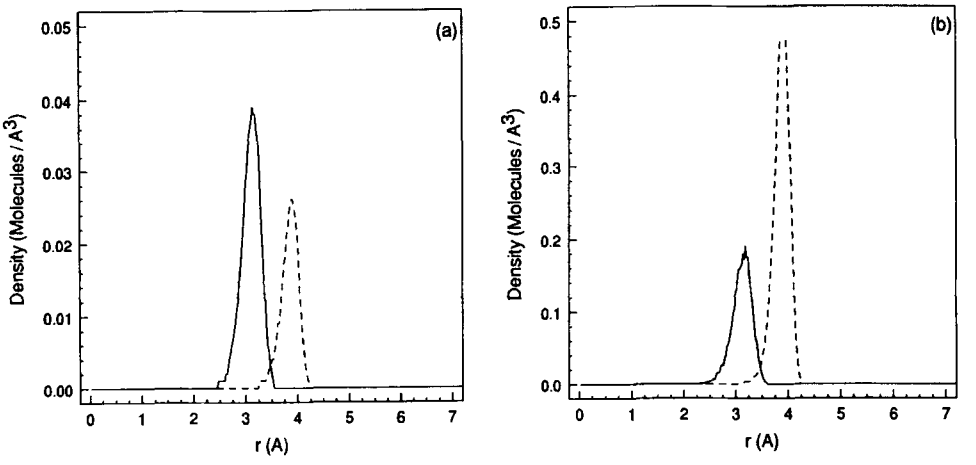

Figure 15 Density profiles as a function of the radius of a 13*X* cavity (– – –) C_2H_4, (——) *i*-C_4H_{10}. (a) Angle-averaged density; (b) Local density at fixed angles facing each of the four sodiums II. ($N_{C_4H_{10}}$ = 2.1, $N_{C_2H_4}$ = 1.9)

Karavias [27]:

$$F = a_1\left[1 - \exp\left(a_2 \frac{\Omega}{kT}\right)\right] \tag{21}$$

The fit is imperfect because of errors in the numerical integration of Equation (17) and some small dependence of F on composition. At $\Omega = 0$, the excess Gibbs free energy is zero and the function F has a finite non-zero slope.

The density profiles of both components are presented in Figure 15. The angle-averaged density of *i*-C_4H_{10} and C_2H_4 at $y_1 = 0.70$, $P = 137.80$ kPa, and $T = 298.15$ K is plotted as a function of the cavity radius in Figure 15a. The components have separate peaks about 1 Å apart. Isobutane is larger than ethylene and therefore is located closer to the center of the cavity. Ethylene, on the other hand, has a larger quadrupole moment interacting with the electric field, which is strongest close to the cavity walls. In Figure 15b, the local density of the two components along solid angles of 0.04 steradians facing the four cations II is plotted. At these positions, ethylene is more strongly adsorbed than isobutane because of the electrostatic interactions. The distribution of the adsorbed molecules inside the cavity is also presented in Figure 16. In this picture, segregation of the two components into different spherical shells is apparent. In addition, the *i*-C_4H_{10} molecules are spread more uniformly inside the cavity than C_2H_4 (see Figure 15).

For the *i*-C_4H_{10}–C_2H_4 binary, the size difference of the adsorbate molecules is primarily responsible for the large negative deviations from ideal behavior. Energetic heterogeneity caused by the electrostatic interactions of the molecules with the zeolite also contributes to the large, negative values of excess Gibbs free energy.

Ideal Adsorbed Solution theory fails to predict multicomponent adsorption equilibrium of molecules with significantly different polarity or size. Molecules with similar single-gas isosteric heat curves behave as ideal solutions, e.g. C_2H_4–CO_2. However, large negative deviations from Raoult's law are found when the structure of the isosteric heat curve is different for the two components [14]. A proper treatment

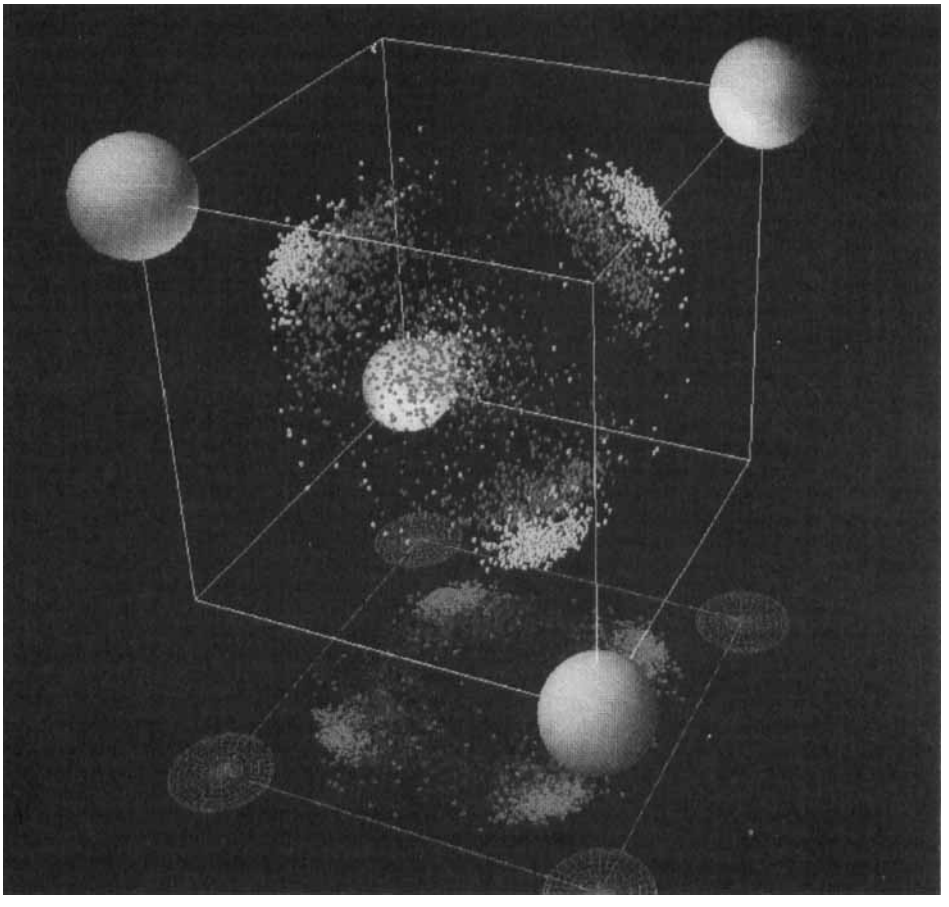

Figure 16 (*See* Color Plate VI) Density distributions of i-C_4H_{10}-C_2H_4 binary in a zeolite cavity of type X. The four cations II are located at the corners of a cube at a distance of 6.8 Å from the center of the cavity. Each spot inside the cube represents the position occupied by the center of mass of the adsorbed molecule at different MC steps. i-C_4H_{10} molecules are green and C_2H_4 molecules are yellow. ($N_{C_4H_{10}} = 2.1$, $N_{C_2H_4} = 1.9$.)

of isosteric heat in the framework of a thermodynamic theory may provide significant information about nonideality that could be applied to improve predictions of multicomponent adsorption.

CONCLUSIONS

Grand canonical Monte Carlo simulations have been performed for binary adsorption of Lennard-Jones molecules with point multipole moments in zeolite cavities of type X. Dispersion–repulsion interactions of adsorbate molecules with the solid were modeled with a spherically-averaged potential. The induced electrostatic potential and the interactions of the point quadrupole moments with the electric field generated

by the zeolite cations were taken into account. The three binary mixtures show a variety of phase behavior: the C_2H_4-CO_2 behaved as an ideal solution, the CO_2-CH_4 showed mild nonidealities, and i-C_4H_{10}-C_2H_4 is highly nonideal.

Phase diagrams and total coverage were calculated for each binary and compared with experimental measurements and predictions of the Ideal Adsorbed Solution theory. Without using any adjustable parameters besides those for single-gas adsorption, MC simulations gave good agreement with experiment for two mixtures (C_2H_4-CO_2 and CO_2-CH_4). There were large discrepancies between simulation and experiment for the system i-C_4H_{10}-C_2H_4.

The grand potential of the MC data was calculated by the Gibbs adsorption equation. The excess Gibbs free energy provides a measure of the deviation of each binary from an ideal solution. The dependence of g^e on the composition and grand potential was studied. Negative deviations from ideality are due to energetic heterogeneity and size effects. Unlike liquid-vapor equilibrium, deviations from the Lorentz-Berthelot mixing rules affect the phase behavior only weakly.

Density profiles of the adsorbed molecules were calculated from the mixture MC simulations. The components compete for the high energy sites; depending on their relative strength of adsorption one component may be excluded from such positions (CH_4 in CO_2-CH_4), or the two species may share sites inside the cavity (C_2H_4-CO_2).

The work presented here shows that MC simulations can be used for predicting multicomponent adsorption equilibria. Moreover, MC sets of data can be used for testing thermodynamic and statistical mechanical theories of adsorption.

Acknowledgements

We thank Dr. N.I. Badler and Welton Becket of the Computer Graphics Research Laboratory, University of Pennsylvania for their help on preparing our color graphics. Support by the Gas Research Institute Contract #5084-260-1254 and by National Science Foundation grant 88-10215 is gratefully acknowledged.

References

[1] K.E. Gubbins, "Simulations of bulk fluid properties", *Molecular Simulation*, **2,** 223 (1989).
[2] A.Z. Panagiotopoulos, U.W. Suter and R.C. Reid, "Phase diagrams of nonideal fluid mixture from Monte Carlo simulation", *Ind. Eng. Chem. Fund.*, **25,** 525 (1986).
[3] A.Z. Panagiotopoulos, N. Quirke, M. Stapleton, and D.J. Tildesley, "Phase equilibria by simulation in the Gibbs ensemble. Alternative derivation, generalization and application to mixture and membrane equilibria", *Mol. Phys.*, **63,** 527 (1988).
[4] M. Nouacer and K.S. Shing, "Grand canonical Monte Carlo simulation for solubility calculation in supercritical extraction", *Molecular Simulation*, **2,** 55 (1989).
[5] G.S. Heffelfinger, Z. Tan, K.E. Gubbins, U. Marconi and F. Van Swol, "Lennard-Jones mixtures in a cylindrical pore. A comparison of simulation and density functional theory", *Molecular Simulation*, **2,** 393 (1989).
[6] J.L. Soto and A.L. Myers, "Monte Carlo studies of adsorption in molecular sieves", *Mol. Phys.*, **42,** 971 (1981).
[7] R.L. June, A.T. Bell and D.N. Theodorou, "Prediction of sorption and diffusion in zeolite catalysts", *J. Phys. Chem.*, **94,** 1508 (1990).
[8] R.Q. Snurr, R.L. June, A.T. Bell and D.N. Theodorou, "Molecular Simulations of Methane Adsorption in Silicalite", AIChE Annual Meeting, Chicago, IL (1990).
[9] G.B. Woods, A.Z. Panagiotopoulos and J.S. Rowlinson, "Adsorption of fluids in model zeolite cavities", *Mol. Phys.*, **63,** 49 (1988).
[10] G.B. Woods and J.S. Rowlinson, "Computer simulations of fluids in zeolite *X* and *Y*", *J. Chem. Soc., Faraday Trans. 2*, **85**(6), 765 (1989).

[11] D.M. Razmus and C.K. Hall, "Prediction of the adsorption of gases in 5A zeolites using Monte Carlo simulations", AIChE Annual Meeting, San Francisco, CA (1989).
[12] S. Yashonath, J.M. Thomas, A.K. Nowak and A.K. Cheetham, "The siting, energetics and mobility of saturated hydrocarbons inside zeolitic cages: methane in zeolite *Y*", *Nature*, **331,** 601 (1988).
[13] S. Yashonath, P. Demontis and M.L. Klein, "Molecular dynamics study of methane in zeolite NaY", *Chem. Phys. Letters*, **153,** 551 (1988).
[14] F. Karavias and A.L. Myers, "Monte Carlo simulations of adsorption of non-polar and polar molecules in zeolite *X*", *Molecular Simulation*, **8,** 23 (1991).
[15] J.L. Soto, P.W. Fisher, A.J. Glessner and A.L. Myers, "Sorption of gases in molecular sieves", *J. Faraday Trans.*, 1, **77,** 157 (1981).
[16] L. Broussard and D.P. Shoemaker, "The structures of synthetic molecules sieves", *J. Am. Chem. Soc.*, **82,** 1041 (1960).
[17] A.D. Buckingham, "Permanent and induced molecular moments and long-ranged intermolecular forces", *Adv. Chem. Phys.*, vol. 12, 107, John Wiley, New York (1967).
[18] M.P. Allen and D.J. Tildesley, *Computer Simulation of Liquids*, Oxford University Press, New York (1987).
[19] D. Nicholson and N.G. Parsonage, *Computer Simulation and the Statistical Mechanics of Adsorption*, Academic Press, New York (1982).
[20] D.A. McQuarrie and J.S. Rowlinson, "The virial expansion of the grand potential at spherical and planar walls", *Mol. Phys.*, **60,** 977 (1987).
[21] J.S. Rowlinson, private communication (1989).
[22] D.P. Valenzuela and A.L. Myers, *Adsorption Equilibrium Data Handbook*, Prentice Hall, New Jersey (1989).
[23] S.H. Hyun and R.P. Danner, "Equilibrium adsorption of ethane, ethylene, isobutane, carbon dioxide, and their binary mixtures on 13*X* molecular sieves", *J. Chem. Eng. Data*, **27,** 196 (1982).
[24] A.L. Myers and J.M. Prausnitz, "Thermodynamics of mixed-gas adsorption", *AIChE J.*, **11,** 1213 (1985).
[25] P.D. Rolniak and R. Kobayashi, "Adsorption of methane and several mixtures of methane and carbon dioxide at elevated pressures and near ambient temperatures on 5A and 13*X* molecular sieves by tracers perturbation chromatography", *AIChE J.*, **26,** 616 (1980).
[26] S. Sircar and A.L. Myers, "Equilibrium adsorption of gases and liquids on heterogeneous adsorbents", *Surf. Sci.*, **205,** 353 (1988).
[27] A.L. Myers and F. Karavias, "Gravimetric Measurements of Adsorption From Gas Mixtures", AIChE Annual Meeting, San Francisco, CA (1989).
[28] R.C. Reid, J.M. Prausnitz and T.K. Sherwood, *The Properties of Gases and Liquids*, McGraw-Hill Book Company, New York (1977).
[29] W.A. Steele, *The Interaction of Gases with Solid Surfaces*, Pergamon Press, Oxford (1974).
[30] J.O. Hirschfelder, C.F. Curtiss and R.B. Bird, *Molecular Theory of Gas and Liquids*, Wiley, New York (1954).
[31] D.E. Strogryn and A.P. Strogryn, "Molecular multipole moments", *Mol. Phys.*, **11,** 371 (1966).
[32] J. Applequist, J.R. Carl and K. Fung, "An atom dipole interaction model for molecular polarizability. Application to polyatomic molecules and determination of atom polarizabilities", *J. Am. Chem. Soc.*, **94,** 2950 (1972).